Regulation of a subset of release-ready vesicles by the presynaptic protein Mover

Ermis Pofantis[a], Erwin Neher[b,c,1], and Thomas Dresbach[a,1]

[a]Institute of Anatomy and Embryology, University Medical Center Göttingen, Georg-August University of Göttingen, 37075 Göttingen, Germany; [b]Emeritus Laboratory of Membrane Biophysics, Max Planck Institute for Biophysical Chemistry, 37077 Göttingen, Germany; and [c]Cluster of Excellence "Multiscale Bioimaging: from Molecular Machines to Networks of Excitable Cells," University of Göttingen, Göttingen, Germany

Contributed by Erwin Neher, December 13, 2020 (sent for review October 29, 2020; reviewed by Edwin R. Chapman and Lu-Yang Wang)

Neurotransmitter release occurs by regulated exocytosis from synaptic vesicles (SVs). Evolutionarily conserved proteins mediate the essential aspects of this process, including the membrane fusion step and priming steps that make SVs release-competent. Unlike the proteins constituting the core fusion machinery, the SV protein Mover does not occur in all species and all synapses. Its restricted expression suggests that Mover may modulate basic aspects of transmitter release and short-term plasticity. To test this hypothesis, we analyzed synaptic transmission electrophysiologically at the mouse calyx of Held synapse in slices obtained from wild-type mice and mice lacking Mover. Spontaneous transmission was unaffected, indicating that the basic release machinery works in the absence of Mover. Evoked release and vesicular release probability were slightly reduced, and the paired pulse ratio was increased in Mover knockout mice. To explore whether Mover's role is restricted to certain subpools of SVs, we analyzed our data in terms of two models of priming. A model assuming two SV pools in parallel showed a reduced release probability of so-called "superprimed vesicles" while "normally primed" ones were unaffected. For the second model, which holds that vesicles transit sequentially from a loosely docked state to a tightly docked state before exocytosis, we found that knocking out Mover selectively decreased the release probability of tight state vesicles. These results indicate that Mover regulates a subclass of primed SVs in the mouse calyx of Held.

synaptic vesicles | presynaptic plasticity | neurotransmission | vesicle priming | Mover

Synaptic transmission is initiated by exocytosis of neurotransmitters from presynaptic nerve terminals. Exocytosis involves tethering of synaptic vesicles (SVs) at release sites, priming to make SVs release-competent, and membrane fusion mediated by Synaptotagmins and SNAREs (1, 2). SVs in the release-competent state constitute the readily releasable pool (RRP) (3). Presynaptic proteins, such as Munc13s, Munc18s, and CAPS, are essential for generating the RRP and for regulating replenishment of this pool during short-term plasticity (4).

Historically, the RRP had been regarded as a uniform set of primed SVs. But more recent evidence suggested that a fraction of SVs in the RRP might be more prone to undergoing exocytosis than others, and these SVs were dubbed "superprimed." In this view, both primed and superprimed SVs are release-competent, albeit with different kinetics (5–7). More recently, evidence emerged that the primed states may be dynamic, reversible, and activity-dependent (8, 9) and they may correlate with morphological features of the synapse (10, 11). Furthermore, molecular evidence indicates that priming proceeds in distinct, reversible steps (12). These reports gave rise to a model which holds that primed SVs fluctuate between a loosely docked state (LS), in which SNARE complexes are partially zippered, and a tightly docked state (TS), in which SNARE zippering has progressed further. In this model, release predominantly occurs from TS vesicles; the transition from LS to TS is slow at rest but can occur rapidly in the presence of Ca^{2+}, on a millisecond time scale (13).

Exocytosis is abolished when components of the core machinery are perturbed, such as Munc13s, Munc18s, or Synaptotagmin-1. However, it is unknown whether there are proteins specifically fine-tuning parts of the priming process. Unlike most presynaptic proteins, the SV protein Mover is not expressed in all species and all synapses (14, 15). Mover is thus a prime candidate for modulating the ubiquitous release machinery. Here, we have tested the role of Mover for modulating synaptic transmission at the calyx of Held. Our data indicate that Mover regulates the release probability (p_r) of a subset of primed SVs.

Results

Spontaneous Transmission Is Unaffected in Mover Knockout. We first recorded spontaneous excitatory postsynaptic potentials (EPSCs) from medial nucleus of the trapezoid body (MNTB) principal neurons in acute brain stem slices obtained from wild-type (WT) and Mover knockout (KO) mice at postnatal days 12 (p12) and 13. We found no significant differences between WT and KO in amplitude, frequency, and kinetics of spontaneous EPSCs, including half width, rise time, and time constants of decay (Fig. 1 *A*–*G*). The lack of an effect on spontaneous synaptic transmission is consistent with the fact that Mover is absent from *Caenorhabditis elegans* and *Drosophila* (14, 15): i.e., Mover is apparently not essential for basic neurotransmission.

Significance

At active zones, ubiquitous proteins tether neurotransmitter-laden vesicles to specialized release sites, make them fusion-competent, and regulate their exocytotic fusion. Can specialized, synapse-specific proteins modulate this machinery? If so, which steps do they regulate? Here, we study mice lacking the presynaptic protein Mover. Mover is absent in some invertebrates and restricted to certain synapses in the rodent brain. Using electrophysiology and mathematical analysis of transmitter release kinetics at the calyx of Held, we find that Mover regulates a subset of fusion-competent synaptic vesicles: Mover selectively affects the vesicles most poised to be released during the initial stages of activity. Thus, by analogy, if ubiquitous proteins are light switches, Mover is a dimmer in transmitter release.

Author contributions: E.P., E.N., and T.D. designed research; E.P. performed research; E.N. contributed new reagents/analytic tools; E.P., E.N., and T.D. analyzed data; and E.P., E.N., and T.D. wrote the paper.

Reviewers: E.R.C., University of Wisconsin–Madison; and L.-Y.W., SickKids Research Institute and University of Toronto.

The authors declare no competing interest.

[1]To whom correspondence may be addressed. Email: eneher@gwdg.de or thomas.dresbach@med.uni-goettingen.de.

Published January 11, 2021.

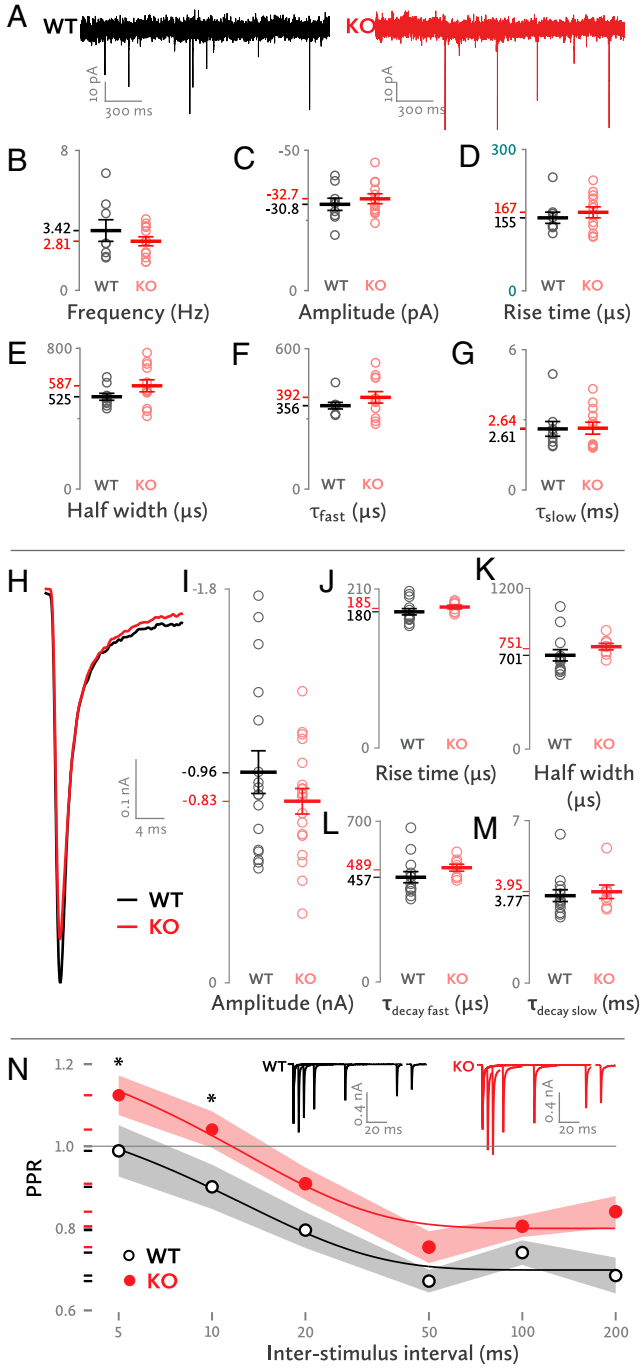

Fig. 1. Basic synaptic transmission properties of the Mover KO. (*A*) Sample traces of spontaneous synaptic transmission. (*B–G*) Properties of spontaneous synaptic activity. Each dot represents one synapse. (*H*) Sample traces of evoked EPSCs for WT and KO synapses. (*I–M*) Properties of evoked EPSCs. (*N*) Paired pulse ratios in various ISIs. Asterisks denote a statistically significant difference. The gray and red shades represent the SEM. (*Inset*) Sample superimposed traces of evoked EPSCs at various ISIs. Each group of traces (WT or KO) belongs to a single cell. Statistics (*B–G*): Frequency: WT: 3.42 ± 0.62 Hz, $n = 8$; KO: 2.81 ± 0.26 Hz, $n = 12$; $t(9.516) = 0.92$; $P = 0.38$; amplitude: WT: −30.75 ± 2.18 pA, $n = 9$; KO: −32.74 ± 1.78 pA, $n = 12$; $t(19) = 0.714$; $P = 0.484$; rise time: WT: 155.09 ± 11.86 µs, $n = 9$; KO: 166.72 ± 11.58 µs, $n = 12$; $t(19) = -0.689$; $P = 0.499$; half width: WT: 524.7 ± 19.91 µs, $n = 9$; KO: 587.15 ± 33.91 µs, $n = 12$; $t(17.098) = -1.588$; $P = 0.131$; τ fast: WT: 356.44 ± 14.09 µs, $n = 9$; KO: 392.38 ± 24.6 µs, $n = 12$; $t(16.897) = -1.267$; $P = 0.222$; τ slow: WT: 2.61 ± 0.32 ms, $n = 9$; KO: 2.64 ± 0.26 ms, $n = 12$; $t(19) = -0.076$; $P = 0.94$.

Increased Paired-Pulse Ratio. Next, we elicited single presynaptic action potentials in afferent fibers and recorded the resulting EPSCs from the postsynaptic principal cell (Fig. 1*H*). We observed a trend toward smaller EPSC amplitudes in KO synapses (Fig. 1*I*) [WT: −0.96 ± 0.098 nA, $n = 17$; KO: −0.83 ± 0.058 nA, $n = 19$; $t(34) = 1.2$; $P = 0.238$]. The EPSC rise time, which is a measure of the synchronicity of synaptic-vesicle fusion, was similar in WT and KO (Fig. 1*J*). EPSC kinetics, including the half width and decay time constants, were also unchanged (Fig. 1 *K–M*). To test whether the initial p_r could be affected, we determined the paired-pulse ratio (PPR): i.e., the ratio of the second EPSC over the first when two closely timed stimuli are given. The KO had a consistently higher PPR, as indicated by a linear mixed-model analysis (Fig. 1*N*) (WT: 0.797 ± 0.022; KO: 0.912 ± 0.02; f(1, 138) = 15.172, $P < 0.001$). Post hoc tests revealed statistically significant differences at 5- and 10-ms interpulse intervals. We conclude that, in Mover's absence, there is a trend toward a reduction of the initial p_r.

Kinetics but Not Extent of Short-Term Depression Are Affected in the KO. A reduced p_r should go along with slower short-term depression. To test this, we stimulated axons with 50-pulse trains, plotted the EPSC amplitudes versus the stimulus number, and fitted these data points with a monoexponential curve (Fig. 2*A*). At frequencies of 5, 10, and 20 Hz, there was no difference in the decay constant τ. At 50 and 100 Hz, the time course of depression was significantly slower at KO synapses than at WT synapses (Fig. 2*B*) (50-Hz trains; WT: τ = 2.78 ± 0.38, $n = 14$; KO: τ = 3.47 ± 0.46, $n = 13$; 100-Hz trains; WT: τ = 3.38 ± 0.33, $n = 15$; KO: τ = 4.24 ± 0.41, $n = 15$; τ units in interstimulus intervals (ISIs); all datasets were fit from the second until the 50th pulse). At 100- and 200-Hz curves, there were systematic deviations from monoexponentiality, pointing to heterogeneity between SV populations addressed in the subsequent paragraphs. In particular, WT 100-Hz stimulation trains were best fit by a monoexponential curve whereas KO 100-Hz and both WT and KO 200-Hz stimulation trains were best fit by double exponential curves. Since the two 100-Hz datasets were each best fit with different models, we chose the simplest of the two that could adequately fit both datasets: i.e., a monoexponential model, to formally compare their decay (Fig. 2*B*). The steady-state levels, determined by the amplitudes of the last 20 EPSCs of each train, were not significantly different between WT and KO synapses at 100 Hz although there was a trend toward higher steady-state levels in the KO (Fig. 2*C*).

RRP Size, Vesicle Replenishment, and p_r. To estimate the size of the RRP and its replenishment, we fit a straight line to the linear part of a cumulative EPSC vs. stimulus number graph, induced by a 100-Hz train; the *y* axis intersection of this straight line reflects the decrement in SV pool content during the train stimulation, and its slope is the replenishment rate of the SV pool (16, 17). Both the RRP and the replenishment rate were marginally increased in the KO calyces (Fig. 2 *D–F*) [RRP; WT: 3.55 ± 0.33 nA, $n = 15$; KO: 3.93 ± 0.34 nA, $n = 15$; $t(28) = -0.806$; $P = 0.427$; replenishment rate; WT: 12.2 ± 1.7 nA/s, $n = 15$; KO: 16.2 ± 1.6 nA/s, $n = 15$; $t(28) = -1.727$; $P = 0.095$]. To test the replenishment rate in the absence of stimulation, we measured the recovery from depression. We induced synaptic depression by 20 stimuli at 100 Hz. Then, at various intervals after the end of the stimulation train, a single EPSC was elicited. The ratio of its amplitude compared with the amplitude of the first EPSC of the train is plotted in Fig. 2*H*. An exponential reaching a plateau was fit to the data, and their growth constant k was compared. No differences were found between WT and KO synapses (WT: $n = 12$; KO: $n = 11$; common k: 0.23 ± 0.03; r^2: 0.997). This indicates that the reloading of the RRP after synaptic depression is unchanged.

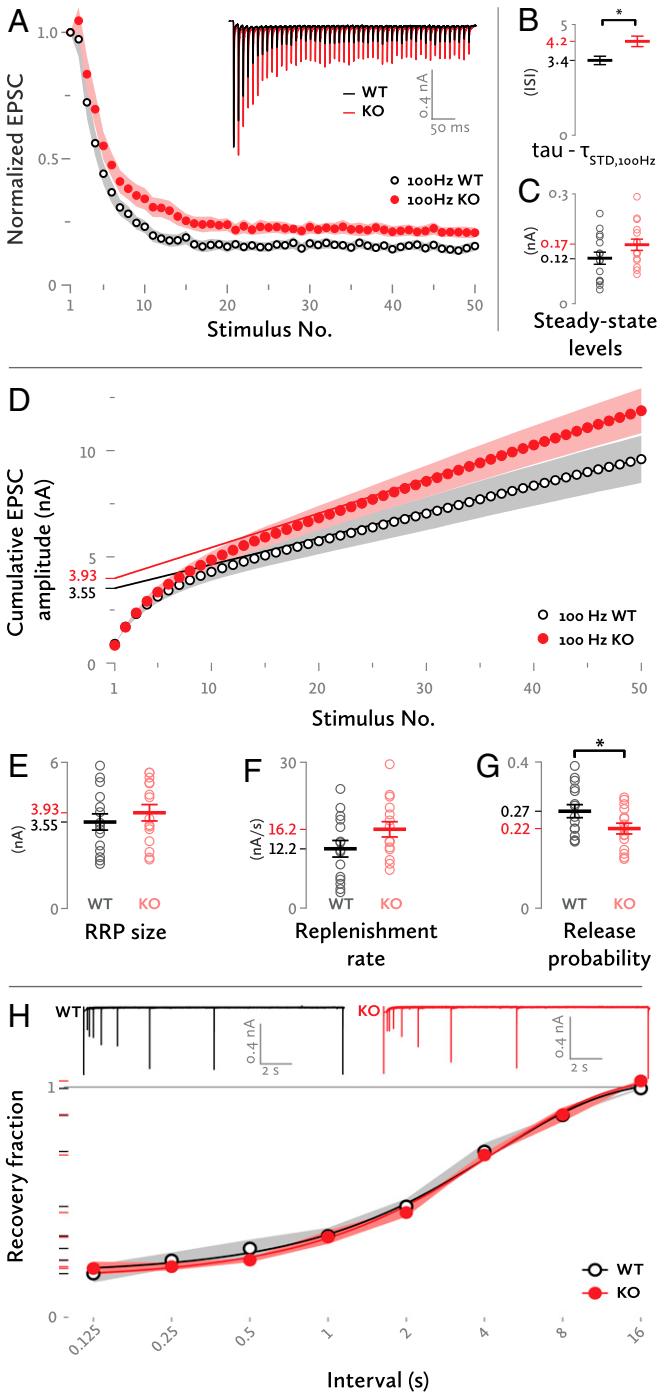

Fig. 2. Short term plasticity. (*A*) Normalized EPSC amplitudes during a 100-Hz stimulation train. A monoexponential curve had a relatively better fit for the WT synapses [extra sum-of-squares F test; F = 1.970 (2,718), $P = 0.14$] whereas the KO synapses were best fit with a double exponential curve [F = 5.972 (2,715), $P = 0.0027$], indicating an underlying heterogeneity of the priming mechanisms. (*Inset*) Sample traces of responses to the same stimulation. (*B*) Time constant of decay (ISI) for the short-term depression (STD) curve of 100 Hz stimulation. The simplest, monoexponential model was chosen to formally compare both groups in the 100-Hz stimulation EPSC amplitude plot. *Difference in Akaike's corrected Information Criterion = 9.5, comparison between a simpler model where tau is the same for both data sets and a complex model where tau is different for each data set. (*C*) Steady-state EPSC amplitude levels for a 100-Hz stimulation train. The values of the last 20 EPSCs of each train were taken into account. Each dot represents one synapse. (*D*) Cumulative plot of EPSC amplitudes during a 100-Hz stimulation train. The regression lines were fit to the last 10 values of each curve and then back-extrapolated to stimulus no. 1. (*E*) RRP size as determined from the point of intersection between the regression lines and the *y* axis. (*F*) Replenishment rate as determined from the slope of the regression lines. (*G*) The p_r of the WT and KO synapses. *$P = 0.05$, independent-samples *t* test. (*H*) Recovery of the EPSC amplitude in various time intervals from a depletion stimulus. (*Inset*) Sample superimposed traces of evoked EPSCs at various intervals after a depletion stimulus. Each group of traces (WT or KO) was recorded from a single cell. The gray and red shades represent the SEM.

The p_r, calculated by dividing the amplitude of the first EPSC over the RRP size, was lower at the KO synapses compared to WT (Fig. 2*G*) [WT: 0.266 ± 0.018, $n = 15$; KO: 0.218 ± 0.015, $n = 15$; $t(28) = 2.048$; $P = 0.05$]. The lower p_r of the KO SVs was due to the combination of two factors: slightly smaller EPSC amplitudes at rest as seen in Fig. 1*I* and a marginally bigger RRP size.

Parallel Release Model: Mover Selectively Affects the Release Probability of the Superprimed SVs. So far, the data provide multiple indications of a reduced p_r in the KO. To test this further, we took into account the increasing evidence for a nonuniform pool of release-competent SVs. A two-SV pool model where both pools release independently from each other was proposed by Taschenberger et al. (6). There, the authors described two states of primed vesicles: a quickly replenished low release probability SV state (normally primed vesicles [SV_n]) and a slowly replenished high release probability state (superprimed vesicles [SV_s]) (Fig. 3*A*).

Each calyx of Held has a specific EPSC amplitude at rest ($EPSC_1$), which differs widely between synapses. This heterogeneity disappears during repetitive high-frequency stimulation. Fig. 3*B* shows an example of two WT cells: one with a high $EPSC_1$ and one with a low $EPSC_1$. Both converge to the same steady-state EPSC levels after four to seven stimulations at 200 Hz. The model postulates that this initial heterogeneity results from different numbers of superprimed SVs in the synapses; these vesicles are rapidly depleted and not sufficiently replenished during a high-frequency train. The low-amplitude, but stationary, EPSCs observed at late stages of a stimulus train are contributed mostly by SV_ns. In order to explain the striking equality of late EPSCs in 200-Hz trains, one may postulate that—in contrast to superprimed SVs—the pool of SV_ns is quite uniform in size between synapses. Contrary to WT cells, KO synapses maintain a small degree of their initial differences in EPSC amplitude even after 20 pulses at 200 Hz (Fig. 3*C*). This may be due to a reduced short-term depression of the superprimed component in KO calyces, or to a small difference in the contributions of normally primed SVs to total release.

Provided that the levels of normally primed SVs are similar among synapses, the cells with the smallest superprimed component will be the ones with the lowest $EPSC_1$. Subtracting these low-$EPSC_1$ cells from the synapses with the highest $EPSC_1$—and thus with the largest SV_s component—removes the normally primed component, leaving almost intact the superprimed one (Fig. 3*D*) (6, 7).

Once isolated, the release probability of the superprimed component (p_s) can be estimated by application of the back-extrapolation method, as used in Fig. 2*D* for the total EPSC amplitudes. This is done by forming the ratio between the initial EPSC value and the *y* axis intersection of a straight line fitted to the last 10 EPSCs of a cumulative plot (cross marks in Fig. 3*D*, where the analysis is illustrated with traces normalized to an initial EPSC value of 1). For the WT synapses, the p_s is 0.47 ± 0.008, and, for the KO, it is 0.35 ± 0.004, indicating a greatly reduced release probability for the SV_ss in the KO synapses.

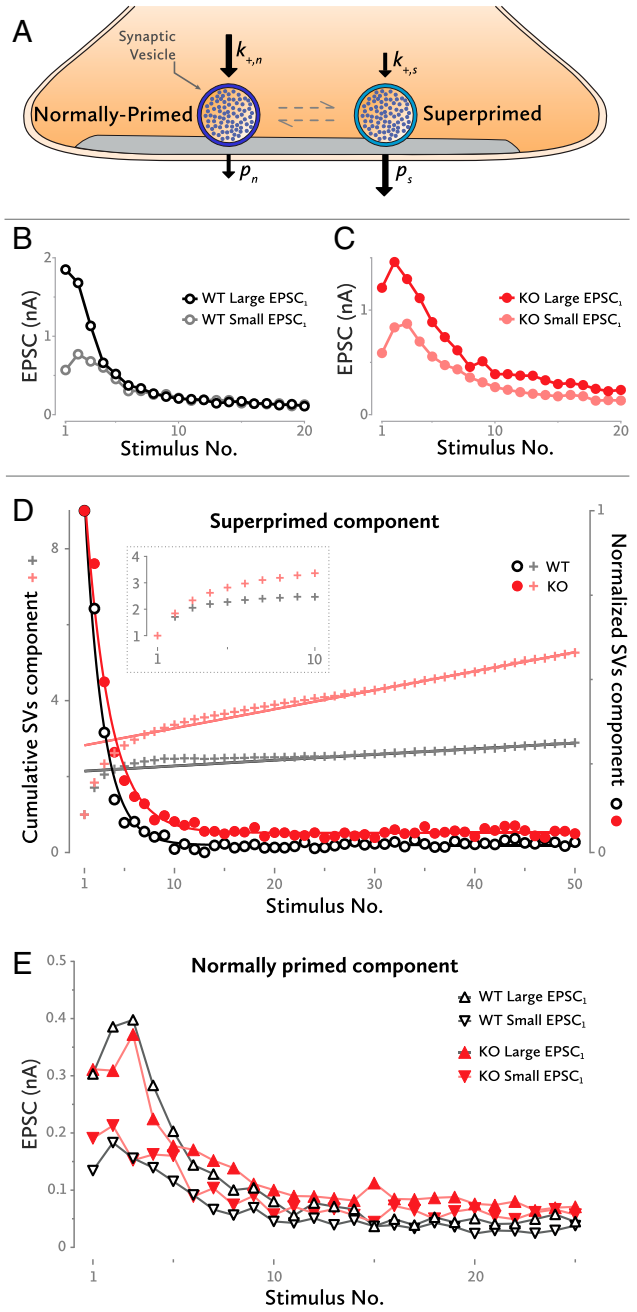

Fig. 3. Superpriming model. (*A*) An SV can be either in the normally primed or in the superprimed state. Each state has its own replenishment rate and release probability. (*B*) Two examples of WT synapses. One has a small initial EPSC amplitude, and the other a large one. Both converge toward the same EPSC levels after a few high-frequency stimulations. (*C*) A similar example for two KO synapses. Even after 20 stimulations, they still retain some degree of their initial differences. (*D*) Isolation of the superprimed component of the EPSC high-frequency trains (circles). The time constant of an exponential fit to the data points is larger for the KO synapses, indicating a lower superprimed SV release probability for that group. Similarly, the *y* axis intersection of a straight line fit to the late data points of the cumulative plot indicates a lower release probability for the superprimed SVs of the KO cells (crosses). The small bump in the cumulative plot between stimulus numbers 5 and 15 is an indication of postsynaptic receptor desensitization, mostly at the high EPSC1 synapses. (*Inset*) The first 10 traces of the cumulative graph, expanded. (*E*) Four representative examples of EPSC trains predepleted by a low-frequency train. All have a similar time constant of decay, indicating a similar range of release probabilities for the normally primed SVs. Although the curves converge to very similar levels, for the given phenotypes, this level is slightly different for WT and KO synapses.

An exponential fit to the time course of the superprimed component can also be used to calculate the p_s; the inverse of the time constant of the fit is equal to the sum of the p_s and the priming rate constant. Since the priming rate of SV_ss at 200 Hz is very small, the inverse of the time constant can be considered almost equal to p_s. For the WT cells, the p_s amounted to 0.55 ± 0.02 whereas, at the KO cells, it was 0.41 ± 0.02. Thus, the KO calyces have again a smaller p_s. The slightly increased p_s values that this method reported could be due to facilitation during the stimulus train; the exponential fit is largely influenced by the steady-state levels whereas the cumulative fit is mostly affected by EPSC amplitudes early in trains.

SV_ss become depressed even during a 10-Hz train, leaving less than 20% of the superprimed pool intact. Furthermore, the time course of the superprimed component (Fig. 3*D*) shows that the SV_s pool is rapidly depleted during a stimulation train. To isolate the SV_ns, a 10-stimuli 10-Hz train was used prior to a 100-Hz stimulus train. Thus, the SV_ss were largely depleted at the beginning of the 100-Hz train, leaving the normally primed SV pool dominating the short-term dynamics. Fig. 3*E* shows examples from two cells for each group, WT and KO. The time courses of the EPSCs contributed by SV_ns are similar irrespective of whether the cell had a low or a high $EPSC_1$, WT or KO; after a few stimulations, the EPSC amplitudes converge. It is noteworthy that the isolated components display pronounced initial facilitation followed by depression whereas total EPSCs often are strictly depressing.

The inverse of the time constant of an exponential fit to an isolated component (measured in units of ISIs) equals to the sum of the release probability of that component and its priming rate constant. In contrast, with the SV_s component, the priming rate of the SV_ns is not negligible and must be taken into account. Hence, only a range of p_n (i.e., the release probability of SV_ns) can be derived from the decay time constant. For both WT and KO SV_ns, similar upper bounds ($p_n < 0.15$) to the p_rs can be estimated. Given that decay time constants as well as estimates for total priming (mainly contributed by SV_ns) are similar, we can conclude that p_n is much smaller than p_s and that it is similar for WT and KO.

Therefore, Mover increases the release probability only of a specific subset of docked and primed SVs: the ones which are ready to be released first upon the arrival of an action potential at a rested synapse.

Sequential Release Model: Mover Selectively Affects the Release Probability of the TS SVs. A minimum release model based on two sequential SV priming steps was proposed by Neher and Brose (13); it involves a TS comprised of SVs which are ready for release at stimulus onset, and an LS, which is considered as the functional precursor of the TS and is comprised of the rest of the SVs docked at release sites. Exocytosis occurs predominantly from the TS pool, and the rate of transition from LS to TS is dependent on intracellular local Ca^{2+} (Fig. 4*A*).

Most current methods for estimating the size of an SV pool cannot distinguish between the LS and TS SV pools (16) since, in this model, the transition from one state to the other is postulated to occur rapidly during high-frequency stimulus trains, which are used for the estimation of pool sizes. Therefore, we explored the predictions regarding differences between WT and KO by a method which allows one to theoretically decompose an EPSC train into its constitutive components. We employed nonnegative tensor factorization (NTF), one of the methods commonly referred to as "blind source separation techniques." NTF reduces high-dimensional data, such as EPSC trains over multiple cells and protocols, into a small number of nonnegative components. These components are an approximate sum of the original data and represent the relative strength of the individual contributions of distinct SV subpools at each point of the

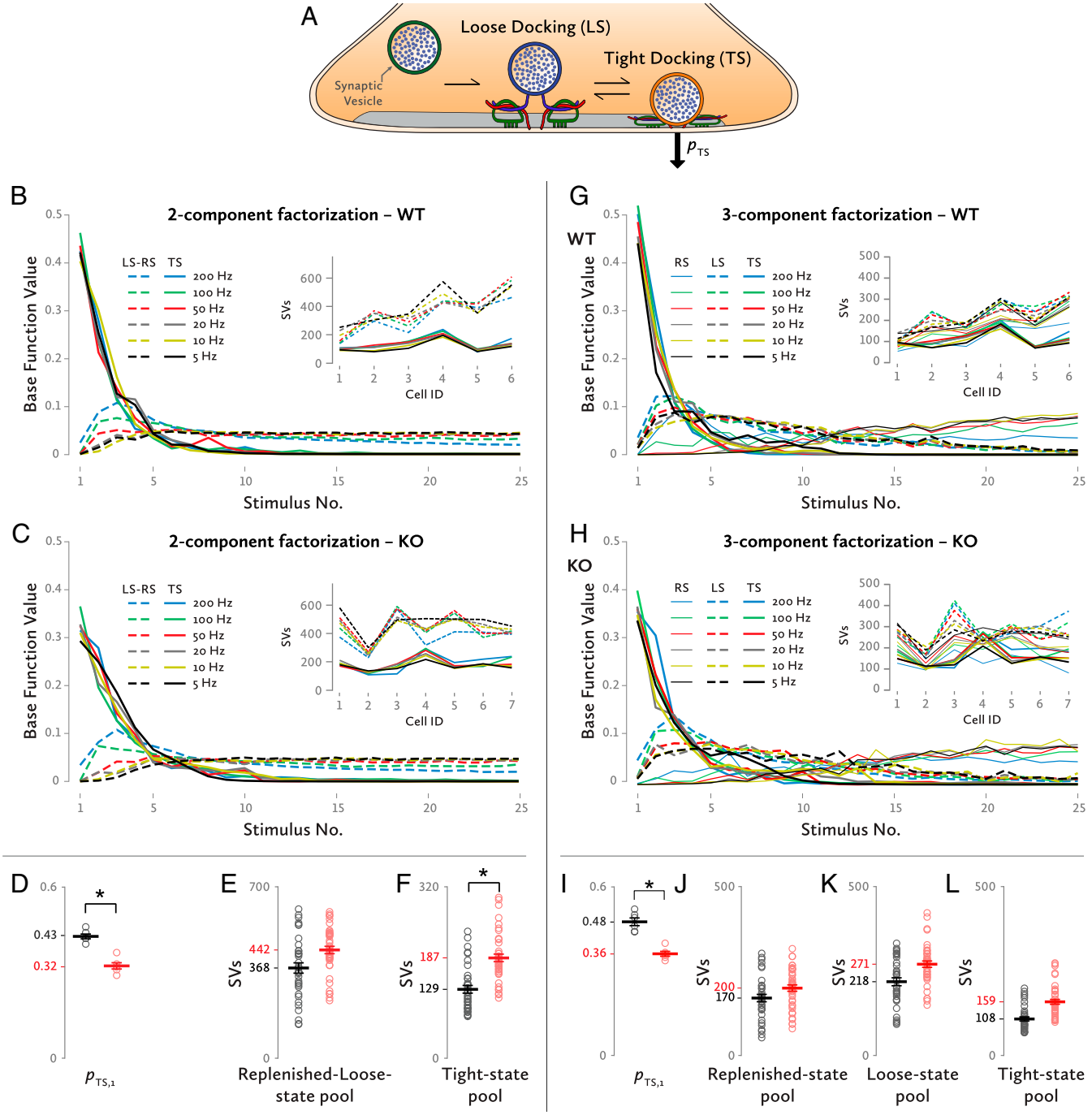

Fig. 4. Analysis by a sequential-release model involving loose and tight docking states of SVs. (*A*) The conformational states an SV can have according to the model. Release occurs only or predominantly from the TS. (*B*) Two-component decomposition at the WT synapses. Solid lines show the component contributed by SVs, which had been in the TS at stimulus onset. Dashed lines indicate the component contributed by SVs, which had been in the loose or recruited state (LS-RS) at stimulus onset. (*Inset*) Pool sizes for the tight-state (solid line) and for the loose- and recruited-state component (dashed line) for each of the synapses that were analyzed. (*C*) Similarly, a two-component decomposition for the KO synapses. (*Inset*) Pool sizes for the TS and LS-RS components for each of the cells that were analyzed. (*D*) The initial release probability of the TS SVs for a two-component decomposition. *$P < 0.0005$, independent-samples *t* test. (*E*) The SV abundances of the RS/LS pools for WT and KO synapses for a two-component decomposition. Each dot represents one frequency stimulation train at one synapse. (*F*) Likewise, sizes of TS pools for WT and KO synapses. Each dot represents train data at a single frequency at one synapse. *$P = 0.033$, two-way mixed ANOVA. (*G*) Three-component decomposition at the WT synapses. Solid lines show the TS component. Dashed lines indicate the LS component while solid thin lines show the RS component. (*Inset*) Pool sizes for the TS (solid lines), for the LS (dashed lines), and RS component (solid thin lines) for each of the synapses that were analyzed. (*H*) Similarly, a three-component decomposition for the KO synapses. (*Inset*) Pool sizes for the TS, LS, and RS components for each of the cells. (*I*) The initial release probability of the TS SVs based on a three-component decomposition [WT: 0.48 ± 0.014, KO: 0.36 ± 0.009, independent-samples *t* test, $t(10) = 7.075$, *$P < 0.0001$]. (*J–L*) The SV abundances of the RS, LS, and TS pools for WT and KO synapses, respectively, for a three-component decomposition. Each dot represents stimulation trains at a single frequency at one synapse: (*J*) WT: 170 ± 22 SVs, KO: 199.6 ± 20.4 SVs, $f(1, 11) = 0.97$, $P = 0.346$, partial $\eta^2 = 0.081$, (*K*) WT: 218.4 ± 26.1 SVs, KO: 270.5 ± 24.2 SVs, $f(1, 11) = 2.139$, $P = 0.172$, partial $\eta^2 = 0.163$, (*L*) WT: 108.2 ± 17.4 SVs, KO: 158.9 ± 16.1 SVs, $f(1, 11) = 4.585$, $P = 0.055$, partial $\eta^2 = 0.294$.

https://doi.org/10.1073/pnas.2022551118

stimulation train for the entire dataset (here called "basefunctions"). Each basefunction is also described by coefficients providing an estimation of the total contribution of each component for each synapse. The approximation is based on the minimization of the error of a least-squares fit to the data under the constraint, that both the vectors and the contributions by individual synapses are nonnegative. It uses an algorithm first described by Lee and Seung (18), as implemented by Neher et al. (19) and Neher and Taschenberger (20).

We first performed an analysis, which separated the EPSC data into two components, one representing the contribution of SVs that had been in the TS at stimulus onset (TS) and a second one, representing all other SVs released during the train (i.e., the sum of SVs, which had been in the LS and those SVs, which undergo the whole sequence of being "R"ecruited, primed, and released). We refer to the latter as LS-RS. In Fig. 4 *B* and *C*, the basefunctions for the TS (BF_{TS}) and LS-RS ($BF_{LS\text{-}RS}$) components are shown for WT and KO animals, respectively. BF_{TS}s are normalized to a cumulative sum of 1. Therefore, their first values are equal to the release probability, $p_{TS,1}$. The KO calyces had a significantly smaller $p_{TS,1}$ (0.32 ± 0.01), when compared to the WT calyces [0.43 ± 0.008 (Fig. 4*D*) independent-samples *t* test, $t(10) = 8.135$, $P < 0.0005$].

NTF also provides an estimation of the size of each component for each synapse. For clarity, the pool sizes estimated in currents were divided by miniature EPSC, the average current produced by a single SV, as shown in Fig. 1*C*; thus, the results are presented in the form of quantal contents of the subpools. The estimation of the TS component's pool size, reveals an almost 50% bigger pool in the KO calyces compared to the WT (Fig. 4*F*); the KO animals' TS pools (187.2 ± 16.4 SVs) were strongly elevated compared to the WT ones [128.5 ± 17.8 SVs, $f(1, 11) = 5.908$, $P = 0.033$, partial $\eta^2 = 0.349$]. The LS-RS component's pool sizes in the KO synapses were only slightly bigger compared to WT synapses (Fig. 4*E*) [WT: 368.1 ± 45 SVs, KO: 441.8 ± 41.6 SVs, $f(1, 11) = 1.446$, $P = 0.254$, partial $\eta^2 = 0.116$].

The morphology of the calyx synapses is likely correlated with their pool size and short-term plasticity: Calyx terminals with relatively simple morphologies display strong short-term depression during a high-frequency stimulation train. In contrast, calyces with complex morphologies have a larger RRP and exhibit initial facilitation which is followed by short-term depression (10). The observed cell-to-cell variations in the LS-RS pool sizes (Fig. 4 *B* and *C*, *Insets*) could be explained based on the inherent variability of the calyx synapses (6). All these findings point to an altered LS-TS balance. Such a difference in balance could be caused by a larger LS-to-TS transition rate in the KO, which would be consistent with the trend toward increased steady-state levels observed in Fig. 2*C*. A lower backward rate from TS to LS (i.e., enhanced stability of TS) would also explain an enhanced LS-TS balance, but not a larger steady-state release at high frequencies.

In an attempt at extracting more information on differences between WT and KO synapses, we ran the NTF analysis once more by decomposing the original dataset into three SV components this time: a recruited one (RS), an LS, and a TS (Fig. 4 *G–L*). Again, the $p_{TS,1}$ was 25% lower for the Mover KO synapses. In accordance with the two-component decomposition results, the pool sizes calculated by the three-component NTF showed an increase of 46.9% for the KO TS pool size. Smaller differences were observed for the LS and the RS SV pools.

The bigger TS pool size in the KO cells together with the lower $p_{TS,1}$ can explain the almost identical $EPSC_1$ amplitudes seen previously in Fig. 1*I*. They can also help explain the slower time course of the 100-Hz train seen in Fig. 2 *A* and *B* since a bigger pool and a lower release probability can result in more SVs being available later on during a stimulation train and thus in a bigger EPSC amplitude. In short, the NTF method provided an estimation of the constitutive components of the EPSC trains. The conclusions reached through this method, i.e., the reduction of the release probability of a subclass of SVs in the KO synapses, again indicate that Mover acts on a subset of release-ready SVs.

Discussion

While the proteins of the core transmitter release machinery are ubiquitous and essential components of synapses, the SV protein Mover is absent from some species: e.g., *C. elegans* and *Drosophila*, and some types of synapses (14, 15). One explanation for this heterogeneous expression of Mover is that it may confer special features to certain synapses, thus allowing these synapses to fine-tune certain aspects of transmitter release. By studying the calyx of Held of mice lacking Mover, we arrived at three key conclusions: first, overall SV p_r was reduced by 18.5% (from 0.27 to 0.22) and the time course of synaptic depression was slower at the calyx of Held of mice lacking Mover compared to WT mice. Second, applying two distinct kinetic models of transmitter release, we found that Mover selectively affects a subset of SVs within the RRP. Third, in both models, Mover boosts the p_r of this subset of docked and primed SVs.

A Subset of Primed SVs Is Affected at the Calyx of Held in Mover KO Mice. The reduced p_r and the slowed time course of depression in our mice are in line with increased facilitation observed at hippocampal mossy fiber terminals in the same mice (21). They are at odds with the increased p_r and faster short-term depression observed upon knockdown of Mover at the rat calyx of Held (22). This difference does not stem from our kinetic models because it is already obvious in the primary recordings, which showed a trend toward a reduced evoked EPSC amplitude in the global KO (this study) versus an increased evoked EPSC amplitude in the knockdown (22). Obviously, there are principal differences in the approaches. For example, Mover is absent throughout development and at all synapses in the KO while the knockdown produced a reduction of Mover levels to approximately 30%, after microinjecting short hairpin RNA (shRNA) at postnatal day 2 selectively into the cochlear nucleus (22). Still, it is hard to imagine how these differences in the experimental approaches would lead to opposite effects on synaptic transmission. One possibility is that differences between the species matter: Even species closely related as the mouse and the rat (23) can have striking differences at the central nervous system level. Differences have been found for cannabinoid receptor effects on the behavior of the animals (24, 25), for the presence or absence of an entire class of synapses, i.e., gap junctions (26), and for expression levels of calcium buffer proteins at the calyx of Held (27). Mover binds to calmodulin and activates calcium/calmodulin/calcineurin signaling (28). Differences in calcium signaling cascades may thus affect the way Mover acts at distinct synapses. Moreover, mice exhibit a remarkable ability to overcome the limitations in sound localization imposed by their relatively small head size. While, in rats, the sound localization threshold closely follows head size, in mice, it does not (29, 30). This could indicate a functional specialization in the auditory pathway present only in mice. Overall, the differences observed in the rat knockdown versus the mouse KO could arise from any one or a combination of reasons, including, 1) distinct developmental adaption mechanisms due to the different perturbation protocols, 2) the difference between complete loss and mere reduction of Mover, and 3) differences between the species. Additional approaches, such as analyzing heterozygous KO mice (assuming that they have reduced Mover levels), analyzing acute Cre-mediated KO of Mover followed by rescue experiments in mice, and analyzing a global KO in rats, are necessary to shed light on the mechanisms that lead to the different outcomes in the two model systems. In any case, we conclude that, in the

Mover KO mouse line studied here, release probability of a subset of primed SVs is reduced at the calyx of Held and, as a result, the time course of short-term depression is slowed.

Two Kinetic Models of Priming Each Reveal Reduced Release Probability of a Subset of Vesicles. Mover is an interesting protein to study because, as a species- and synapse-specific molecule, it may fine-tune transmitter release and short-term plasticity. As expected for a modulating protein, the effects of its loss on release were subtle, under the assumption of a homogeneous pool of release-ready SVs. Previous work has reported different subsets of SVs mediating transmission at various synapses. For example, fast releasing and slow releasing SVs have been identified at the calyx of Held (31). At cerebellar granule cell to basket cell synapses, the active zone protein Munc13-3 appears to superprime release-ready SVs (32). At synapses between presynaptic parallel fibers and postsynaptic molecular-layer interneurons, a well-synchronized component of release mediated the first AP at the onset of burst-like activity. During bursts of activity, however, a slow, desynchronized component gradually took over. A sequential release model was sufficient to explain the observed data (33).

Overall, there is increasing evidence that primed SVs are heterogeneous in their properties (13). Considering the simplest case, i.e., that there are two primed SV states, one can distinguish two classes of models: 1) the states could be arranged in parallel, assuming two kinds of SV states both of which can release independently; and 2) the states could be arranged sequentially, such that any SV has to transit between them, with only SVs in the fully primed state being able to release transmitter. The parallel model assumes one population of primed SVs with high release probability (high-p SVs) and slow priming, and another population with lower probability (low-p SVs) and fast priming. For the calyx of Held, this model had been introduced as the superpriming model of SV release (34). In the sequential model, only the fully primed state is release-competent, and it is replenished in an activity-dependent manner from SVs in the partially primed state, in which they are unable to fuse. In this model, the fully primed SVs have been described as TS vesicles and the partially-primed state as LS, referring to the state of assembly of their SNARE complex proteins (13).

Because the two scenarios cannot be readily distinguished experimentally, we analyzed our data in terms of the two extremes (i.e., fully parallel and fully sequential). The well-characterized physiology of the calyx of Held allowed us to apply specific stimulation protocols, followed by kinetic analysis to analyze the data in the context of the two models. This revealed more pronounced effects of Mover on a certain SV subpopulation in both scenarios: Specifically, the release probability estimations for the superprimed and the TS subpool each showed a reduction in the release probability of ~26% in the absence of Mover. Remarkably, both the parallel and the sequential model yielded virtually identical reductions in release probability for the superprimed pool (25.53 and 25.45%) and the TS pool (25.58%). This reduction contrasts with only 18% reduction in the overall p_r as calculated on the 100-Hz stimulation train EPSCs by the extrapolation method, which makes no distinction between SV subpools.

Our analysis of the parallel model in terms of two pools of SVs with different properties does not specify what the mechanisms underlying these differences are. However, a recent publication (11) demonstrates heterogeneity among SVs at the mouse calyx of Held, with properties of subpools similar to those described here: The stalk-like compartments of terminals, described in this study, harbor SVs with higher p_r and shorter coupling distance to Ca^{2+} channels while bouton-like swellings harbor SVs with lower p_r and longer coupling distance. The filamentous protein septin 5 appears to promote higher p_r and tightness of coupling. Thus, septin-dependent control of p_r via regulation of Ca^{2+} channel-SV coupling may well be the reason for heterogeneity between subpool properties described here. It will be interesting to explore if Mover is more abundant in stalks versus swellings and how it may interact with septins.

In both the parallel and the sequential scenario, the SVs that dominate release either in stand-alone EPSCs or during the initial stages of a high-frequency train were the ones affected by the lack of Mover. Thus, both models indicate that Mover selectively—or at least primarily—affects the subpool of SVs most poised to be released when the synapse is at rest. Of note, the two models are not mutually exclusive. They are merely two extreme scenarios, i.e., strictly parallel and strictly sequential, of the steps underlying SV priming, and they do not exclude the possibility that a continuum of the two scenarios operates at synapses. In both models, Mover affects the subpopulation of SVs that determine release during a single evoked event and early during trains of stimuli. In the parallel model, these are the high-p SVs. In the sequential model, these are the SVs that are in TS at stimulus onset. In summary, two models of priming each reveal pronounced effects of Mover on a subpopulation of SVs, and these SVs have similar roles for transmitter release in the two models.

Compensatory Effects. Knocking out Mover increased the PPR and slowed the time course of short-term depression. This is reminiscent of the effects of knocking out Mover at the hippocampal mossy fiber terminal, which also increased the PPR and, in addition, increased low-frequency facilitation (21). Thus, the calyx of Held and the hippocampal mossy fiber terminal showed a change in short-term plasticity in the same direction, and the phenotypes are consistent with reduced p_r. In particular, the reduced release probability of superprimed vesicles and the reduced release probability of TS vesicles, depending on the model, each are sufficient to explain the increased PPR and slowed depression.

While both models indicate a reduced release probability of a subclass of SVs, they also revealed evidence for compensatory events. In the sequential model, compensation was apparent as an increase in the TS pool size. Of note, this increase did not occur at the expense of the LS-RS pool, which was unchanged, pointing to an overall increase in the number of primed SVs. The parallel model, on the other hand, cannot predict individual subpool sizes (6). However, the RRP estimation obtained through the back-extrapolation method reported a trend toward an increase in the overall RRP size, thus corroborating the sequential model predictions. As a result of this increase, the size of the first EPSC was not affected. The increased TS pool counteracts both the reduced release probability and the slowing of the time course of depression. Thus, we may be underestimating the extent of the effect of Mover on release.

These considerations require caution because we cannot exclude that the primary effect of knocking out Mover is an increase in TS occupancy and that the reduction of TS release probability is the compensatory mechanism. However, according to the sequential model, a larger TS pool would entail faster depression (13). Because we observe the opposite, i.e., slowed depression, this scenario would require an additional assumption: i.e., that the increase in TS occupancy is overcompensated for by a reduction in TS release probability to an extent that short-term depression is slowed. Although this scenario is not impossible, it entails an additional assumption, rendering it less compelling.

Toward a Molecular Scenario. In the minimal LS vs. TS model described by Neher and Brose (13), Munc13s and Synaptotagmins are candidates for regulating the LS/TS transition because they are regulated by calcium and they are part of the

priming machinery. However, if these proteins regulate the LS/TS transition, this is only part of their functions and may in fact represent an inevitable aspect of their essential priming actions (35). The abolition of SNARE proteins, Munc13-1, Munc18-1, or Synaptotagmin-1 results in the total collapse of synchronous release. The removal of Mover, on the other hand, deregulates finer aspects of priming: the release probability and relative abundance of TS vesicles. Generating the fully primed state appears to be a reversible reaction, with Munc13-1 and Munc18-1 being required to prevent "de-priming." In addition, calcium—potentially via binding to Munc13-1—promotes the maintenance of the fully primed state. In the absence of Munc13-1 or Munc18-1, SVs relapse into a nonreleasable state (8). While Munc13-1, Munc18-1, Syt1 (9), and CAPS (36, 37) are essential for generating and maintaining the fully primed state, Mover may modulate their roles in the priming/depriming reaction. Mover binds to CaM and activates CaM/Calcineurin signaling upon heterologous expression (28). In addition, Mover binds to a C-terminal area of Bassoon (14), which is located approximately 50 nm from the center of the synaptic cleft (38): i.e., where docked SVs reside. Thus, Bassoon could direct Mover to its site of action, and CaM binding could confer calcium dependence to Mover. Our data also show that occupancy and release probability of TS SVs can be experimentally differentiated and that they are differentially affected by knocking out Mover. Thus, the calyx of Held is endowed with a remarkable capacity for fine-tuning the final stages of transmitter release.

Materials and Methods

KO Line Generation. The global Mover KO line was generated as described (21, 28). Briefly, conditional KO mice carrying loxP sites upstream of exon 1 and downstream of exon 3 of Mover were crossed with mice expressing Cre recombinase under the E2A promoter to generate a global Mover KO. The KO was verified by sequencing and Western blotting (21, 28). For genotyping, WT and KO animals were identified by the presence of a specific 867-base pair (bp) and a 697-bp band, respectively.

Slice Preparation. Juvenile (p12 to p13) littermate mice (*Mus musculus*) of either sex were used. All experiments complied with the German Protection of Animals Act and with the guidelines for the welfare of experimental animals issued by the European Communities Council Directive. Following decapitation, the whole brain was immersed in low-Ca^{2+} artificial cerebrospinal fluid (ACSF) containing (in mM) 125 NaCl, 2.5 KCl, 25 $NaHCO_3$, 1.25 NaH_2PO_4, 10 glucose, 0.4 ascorbic acid, 3 myo-inositol, 2 Na-pyruvate, 3 $MgCl_2$, and 0.1 $CaCl_2$ (osmolality 308 to 312 mOsm/kg), bubbled continuously with carbogen (95% O_2, 5% CO_2) and kept at 4 °C. The brain stem was then cut in 275-μm-thick slices with a vibratome (Microm HM 650V, Thermo Scientific). The slices were subsequently incubated in normal ACSF at 35 °C for 30 to 45 min and at room temperature (22.5 ± 1 °C). The normal ACSF differed from the low-Ca^{2+} ACSF only in the following (in mM): 1 $MgCl_2$ and 2 $CaCl_2$.

Electrophysiology. Slices were placed in a submerged-type chamber and were continuously perfused at 1 to 1.5 mL/min with carbogen-saturated ACSF and kept at 25 °C. For stimulating the bushy-cell axons innervating the medial nucleus of the trapezoid body principal cells, a parallel bipolar electrode (cat. no. PBSA0275; FHC) was placed close to midline and was used to deliver electrical pulses through an isolated current stimulator (model DS3; Digitimer).

Postsynaptic recordings were performed using pipettes with an open tip resistance of 1.6 to 2.6 MΩ and filled with solution containing (in mM): 10 KCl, 130 K-gluconate, 10 4-(2-hydroxyethyl)-1-piperazineethanesulfonic acid (HEPES), 10 Tetraethylammonium chloride (TEA-Cl), 5 Na_2-phosphocreatine, 5 ethylene glycol bis(β-aminoethyl ether)-*N*,*N*,*N*′,*N*′-tetraacetic acid (EGTA), 4 Mg- adenosine 5′-triphosphate (ATP), 0.3 Na_2- guanosine 5′-triphosphate (GTP) (pH 7.2, osmolality 300–303 mOsm/kg). In all evoked-release recordings, the ACSF was supplemented with 2 mM kynurenic acid. Cells were clamped at −70 mV, and series resistance was 3 to 6.5 MΩ, which was compensated for as much as it was possible without the clamp becoming unstable. Spontaneous postsynaptic currents were recorded without series compensation. Current leak was less than −50 pA.

Blocking presynaptic APs by 1 μM Tetrodotoxin (TTX) does not affect the amplitude or the frequency of spontaneous EPSCs at the calyx of Held (39). Thus, spontaneous EPSCs, recorded in the absence of TTX, do not result from multiquantal events caused by spontaneous APs but represent spontaneous release of transmitter at this synapse (40).

Statistical Analysis. Electrophysiological data were analyzed using custom procedures in IGOR Pro (Wavemetrics). Statistical analysis was performed using SPSS Statistics (IBM) and Prism (GraphPad Software). Statistical significance was determined using independent-samples *t* test except where otherwise noted. Data are presented as mean and SE of mean (SEM). The NTF analysis was performed in IGOR Pro using custom routines.

NTF Analysis. The dataset was comprised of 13 cells in total; 6 cells from WT and 7 from KO animals. Every cell was stimulated with 25-pulse trains at 200, 100, 50, 20, 10, and 5 Hz. Additionally, the synapses were also stimulated with a 200-Hz train preceded by two conditioning pulses at 10 Hz. The conditioning stimuli were used as a way to deplete the TS vesicle pool without large effects on the other components, similar to the superpriming model previously used in this study. Separate NTF runs for every frequency were performed: one NTF analysis for the 200-Hz trains and its predepleted variant, another NTF for the 100-Hz trains, and so on. By normalizing the TS basefunction's integral to 1, its initial value corresponds to the release probability ($p_{TS,1}$). Additionally, the $p_{TS,1}$ should be independent of subsequent stimulation frequency. Therefore, it was constrained at retaining similar values between the different NTF runs.

Likewise, the number of assigned SVs to the TS and LS pools should be independent of subsequent stimulation. Hence, the NTF solutions were confined to achieving similar pool sizes between runs for the various frequency trains. A detailed description of the use of the NTF tool for the decomposition of EPSC trains can be found in Neher and Taschenberger (20).

All experiments involving animals complied with guidelines issued by the State Government of Lower Saxony, Germany, and were approved by the University Medical Center Göttingen Board for Animal Welfare.

Data Availability. All study data are included in the article.

ACKNOWLEDGMENTS. E.N. acknowledges associate membership in the Collaborative Research Center "Quantitative Synaptology" (SFB 1286) of the Deutsche Forschungsgemeinschaft (DFG). This work was supported by the DFG via the Collaborative Research Center 889 (T.D.). We thank Irmgard Weiss for technical assistance. Portions of this work featured in the dissertation of E.P., which was published in 2019 (41).

1. T. C. Südhof, The presynaptic active zone. *Neuron* **75**, 11–25 (2012).
2. T. C. Südhof, Neurotransmitter release: The last millisecond in the life of a synaptic vesicle. *Neuron* **80**, 675–690 (2013).
3. S. M. Wojcik, N. Brose, Regulation of membrane fusion in synaptic excitation-secretion coupling: Speed and accuracy matter. *Neuron* **55**, 11–24 (2007).
4. R. S. Zucker, W. G. Regehr, Short-term synaptic plasticity. *Annu. Rev. Physiol.* **64**, 355–405 (2002).
5. R. Xue *et al*., Doc2-mediated superpriming supports synaptic augmentation. *Proc. Natl. Acad. Sci. U.S.A.* **115**, E5605–E5613 (2018).
6. H. Taschenberger, A. Woehler, E. Neher, Superpriming of synaptic vesicles as a common basis for intersynapse variability and modulation of synaptic strength. *Proc. Natl. Acad. Sci. U.S.A.* **113**, E4548–E4557 (2016).
7. O. M. Schlüter, J. Basu, T. C. Südhof, C. Rosenmund, Rab3 superprimes synaptic vesicles for release: Implications for short-term synaptic plasticity. *J. Neurosci.* **26**, 1239–1246 (2006).
8. E. He *et al*., Munc13-1 and Munc18-1 together prevent NSF-dependent de-priming of synaptic vesicles. *Nat. Commun.* **8**, 15915 (2017).
9. S. Chang, T. Trimbuch, C. Rosenmund, Synaptotagmin-1 drives synchronous Ca^{2+}-triggered fusion by C_2B-domain-mediated synaptic-vesicle-membrane attachment. *Nat. Neurosci.* **21**, 33–40 (2018).
10. G. Grande, L. Y. Wang, Morphological and functional continuum underlying heterogeneity in the spiking fidelity at the calyx of Held synapse in vitro. *J. Neurosci.* **31**, 13386–13399 (2011).
11. A. Fekete *et al*., Underpinning heterogeneity in synaptic transmission by presynaptic ensembles of distinct morphological modules. *Nat. Commun.* **10**, 826 (2019).
12. M. T. Palfreyman, E. M. Jorgensen, Unc13 aligns SNAREs and superprimes synaptic vesicles. *Neuron* **95**, 473–475 (2017).
13. E. Neher, N. Brose, Dynamically primed synaptic vesicle states: Key to understand synaptic short-term plasticity. *Neuron* **100**, 1283–1291 (2018).
14. T. Kremer *et al*., Mover is a novel vertebrate-specific presynaptic protein with differential distribution at subsets of CNS synapses. *FEBS Lett.* **581**, 4727–4733 (2007).
15. R. Wallrafen, T. Dresbach, The presynaptic protein mover is differentially expressed across brain areas and synapse types. *Front. Neuroanat.* **12**, 58 (2018).

16. E. Neher, Merits and limitations of vesicle pool models in view of heterogeneous populations of synaptic vesicles. *Neuron* **87**, 1131–1142 (2015).
17. R. Schneggenburger, A. C. Meyer, E. Neher, Released fraction and total size of a pool of immediately available transmitter quanta at a calyx synapse. *Neuron* **23**, 399–409 (1999).
18. D. D. Lee, H. S. Seung, Learning the parts of objects by non-negative matrix factorization. *Nature* **401**, 788–791 (1999).
19. R. A. Neher *et al*., Blind source separation techniques for the decomposition of multiply labeled fluorescence images. *Biophys. J.* **96**, 3791–3800 (2009).
20. E. Neher, H. Taschenberger, Non-negative matrix factorization as a tool to distinguish between synaptic vesicles in different functional states. *Neuroscience* (2020).
21. J. S. Viotti, T. Dresbach, Differential effect on hippocampal synaptic facilitation by the presynaptic protein mover. *Front. Synaptic Neurosci.* **11**, 30 (2019).
22. C. Körber *et al*., Modulation of presynaptic release probability by the vertebrate-specific protein mover. *Neuron* **87**, 521–533 (2015).
23. R. A. Gibbs *et al*.; Rat Genome Sequencing Project Consortium, Genome sequence of the Brown Norway rat yields insights into mammalian evolution. *Nature* **428**, 493–521 (2004).
24. A. F. Hoffman, A. M. Macgill, D. Smith, M. Oz, C. R. Lupica, Species and strain differences in the expression of a novel glutamate-modulating cannabinoid receptor in the rodent hippocampus. *Eur. J. Neurosci.* **22**, 2387–2391 (2005).
25. J. Haller *et al*., Correlated species differences in the effects of cannabinoid ligands on anxiety and on GABAergic and glutamatergic synaptic transmission. *Eur. J. Neurosci.* **25**, 2445–2456 (2007).
26. S. Stagkourakis, C. T. Pérez, A. Hellysaz, R. Ammari, C. Broberger, Network oscillation rules imposed by species-specific electrical coupling. *eLife* **7**, e33144 (2018).
27. F. Felmy, R. Schneggenburger, Developmental expression of the Ca2+-binding proteins calretinin and parvalbumin at the calyx of Held of rats and mice. *Eur. J. Neurosci.* **20**, 1473–1482 (2004).
28. A. K. Akula *et al*., The calmodulin binding region of the synaptic vesicle protein mover is required for homomeric interaction and presynaptic targeting. *Front. Mol. Neurosci.* **12**, 249 (2019).
29. R. S. Heffner, H. E. Heffner, Sound localization in a predatory rodent, the northern grasshopper mouse (Onychomys leucogaster). *J. Comp. Psychol.* **102**, 66–71 (1988).
30. G. Ehret, A. Dreyer, Localization of tones and noise in the horizontal plane by unrestrained house mice (Mus musculus). *J. Exp. Biol.* **109**, 163–174 (1984).
31. Z. Chen, B. Das, Y. Nakamura, D. A. DiGregorio, S. M. Young Jr, Ca2+ channel to synaptic vesicle distance accounts for the readily releasable pool kinetics at a functionally mature auditory synapse. *J. Neurosci.* **35**, 2083–2100 (2015).
32. S. Ishiyama, H. Schmidt, B. H. Cooper, N. Brose, J. Eilers, Munc13-3 superprimes synaptic vesicles at granule cell-to-basket cell synapses in the mouse cerebellum. *J. Neurosci.* **34**, 14687–14696 (2014).
33. T. Miki, Y. Nakamura, G. Malagon, E. Neher, A. Marty, Two-component latency distributions indicate two-step vesicular release at simple glutamatergic synapses. *Nat. Commun.* **9**, 3943 (2018).
34. J. S. Lee, W. K. Ho, E. Neher, S. H. Lee, Superpriming of synaptic vesicles after their recruitment to the readily releasable pool. *Proc. Natl. Acad. Sci. U.S.A.* **110**, 15079–15084 (2013).
35. J. S. Dittman, Unc13: A multifunctional synaptic marvel. *Curr. Opin. Neurobiol.* **57**, 17–25 (2019).
36. C. Imig *et al*., The morphological and molecular nature of synaptic vesicle priming at presynaptic active zones. *Neuron* **84**, 416–431 (2014).
37. W. J. Jockusch *et al*., CAPS-1 and CAPS-2 are essential synaptic vesicle priming proteins. *Cell* **131**, 796–808 (2007).
38. A. Dani, B. Huang, J. Bergan, C. Dulac, X. Zhuang, Superresolution imaging of chemical synapses in the brain. *Neuron* **68**, 843–856 (2010).
39. T. Ishikawa, Y. Sahara, T. Takahashi, A single packet of transmitter does not saturate postsynaptic glutamate receptors. *Neuron* **34**, 613–621 (2002).
40. R. Schneggenburger, I. D. Forsythe, The calyx of Held. *Cell Tissue Res.* **326**, 311–337 (2006).
41. E. Pofantis, *Mover affects a subpool of primed synaptic vesicles in the mouse calyx of Held* (Georg-August-Universität Göttingen, Göttingen, Germany, 2019).